Supporting Information

Synergistic Enhancement of Photocatalytic Hydrogen Evolution in $ZnIn_2S_4/CuWO_4$ via S-Scheme Heterojunction and Photothermal Effect

Dafeng Zhang[a], Dong Zhang[b], Fuping Zhao[a], Yutong Zhao[a], Hengshuai Li[b,*], Junchang Liu[a,*], Xue-Yang Ji[a], Xipeng Pu[a], Huayang Zhang[c,*]

[a]School of Materials Science and Engineering, Shandong Provincial Key Laboratory of Chemical Energy Storage and Novel Cell Technology, Liaocheng University, Liaocheng, 252000, P. R. China
[b]School of Physics Science and Information Technology, Shandong Key Laboratory of Optical Communication Science and Technology, Liaocheng University, Liaocheng, 252000, P. R. China
[c]School of Chemical Engineering, The University of Adelaide, Adelaide, South Australia, 5005, Australia
*Corresponding author:
E-mail address: lihengshuai@lcu.edu.cn (H. Li), liujunchang@lcu.edu.cn (J. Liu), huayang.zhang@adelaide.edu.au (H. Zhang)

1.1. Characterizations

X-ray diffraction (XRD) patterns were obtained from a Bruker D8 Advance spectrometer (Bruker Co., Germany) using Cu-Kα radiation. Raman spectra were recorded on a LabRAM HR Evolution The morphologies of samples were characterized on a Gemini scanning electron microscope (SEM; Zeiss Ltd., Germany) and a JEM-2100 microscope (TEM; JEOL Ltd., Japan). The content and distribution of elements were determined using an INCA energy spectrometer (EDS; Oxford Instruments, United Kingdom). X-ray photoelectron spectroscopy (XPS) was performed using a K-Alpha system (Thermo Fisher Scientific Ltd., USA). The zeta potentials of the samples were tested on a Nano ZS Zetasizer (Malvern Co., United Kingdom). Absorbance spectra (UV–vis DRS) of samples were obtained by a UV-3600 spectrophotometer (Shimadzu, Japan). Fluorescence spectrometry (PL) for samples was measured using an FLS 920 fluorescence and phosphorescence spectrometer (Edinburgh Co., United Kingdom).

The electron spin resonance (ESR) spectra were measured on CIQTEK EPR200-Plus (CIQTEK Co., Ltd., China) with continue-wave X band frequency.

1.2. Photocatalytic measurement

The photochemical measurements were performed using a standard three-electrode system on a 660E electrochemical workstation (Shanghai Chenhua Co., China), with a platinum wire as the auxiliary electrode and a saturated calomel electrode (SCE) as the reference electrode. The working electrode was prepared as follows: 10 mg photocatalyst was suspended in 1 mL isopropanol-water (4:1) solution and sonicated for 10 min, and then 30 μL of the obtained slurry was injected into a 0.25 cm^2 SnO_2: F (FTO) glass electrode and dried. Finally, the photocurrent, electrochemical impedance spectra (EIS) and Mott-Schottky (M-S) plots were measured under visible light in 0.1 M Na_2SO_4 aqueous solution using a Ceaulight 300 W Xenon lamp.

1.3. Photocatalytic hydrogen evolution test

The photocatalytic hydrogen evolution experiments were carried out in a 250 mL sealed quartz reactor with a constant temperature system of 6 °C. The procedure was as follows: firstly, 20 mg of photocatalyst was dispersed into 100 mL of solution with 0.25 M Na_2SO_3 and 0.35 M Na_2S. Secondly, after sonication for 10 min and degassing for 30 min, a 300 W Xe lamp with a filter ($\lambda > 400$ nm) was turned on to irradiate the reactor. The evolved H_2 was quantified every 30 min using an online gas chromatograph (CEL-SPH2N-D9, Beijing China Education Au-light Co.). In addition, the apparent quantum efficiency (AQE) at 420 (450, 500 and 600) nm under conditions of a 16 cm^2 irradiation area.

1.4. Computational details

First-principle calculations were based on density functional theory (DFT) with CASTEP and DMol3 packages of Materials Studio. The generalized gradient approximation (GGA) was used to deal with the

electron-electron interactions, and the Perdew-Burke-Ernzerhof (PBE) function was used to deal with the exchange correlation. The thickness of the air layer was set to 15 Å to avoid the mutual influence between layers. The distance between CWO and ZIS was set to 3 Å to form a ZIS/CWO heterojunction. The Gibbs free energy ΔG_{H*} was calculated to evaluate the computational high-throughput screening of photocatalytic materials for H_2 evolution:

$$\Delta G_{H*} = \Delta E_H + \Delta_{ZPE} - T\Delta S_H, \Delta E_H = E_{H*} - E_{(catalyst)} - \frac{1}{2}E_H$$

where ΔE_H represents the hydrogen adsorption energy, where E_{H*}, $E_{(catalyst)}$ and E_H are the energies for the H* adsorption on catalyst surface, catalyst, and hydrogen, respectively; ΔE_{ZPE} represents the change in zero-point energy; T is the absolute temperature (298.15 K), and ΔS_H denotes the change of entropy.

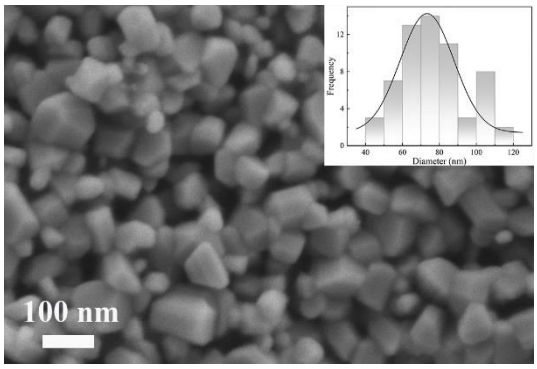

Fig. S1. SEM images and diameter distribution histogram of CWO.

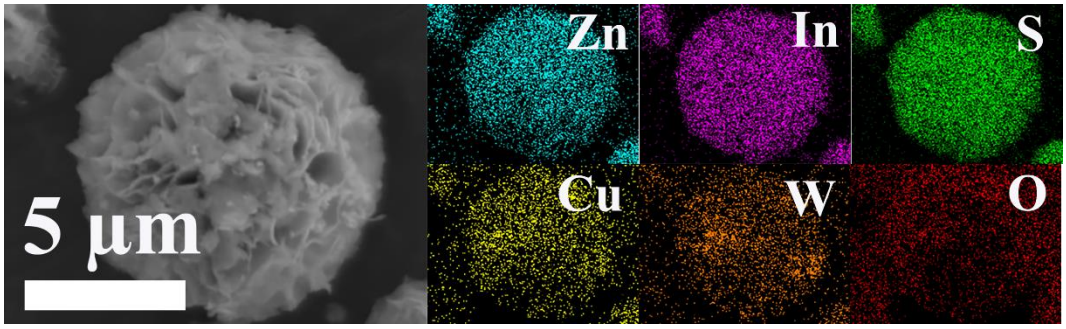

Fig. S2. (a) EDS spectrum of ZIS/CWO-3.

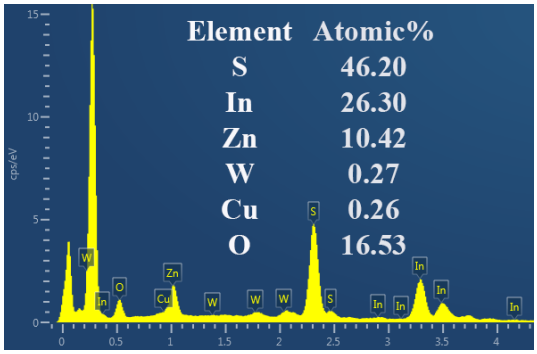

Fig. S3. Elemental mapping of ZIS/CWO-3

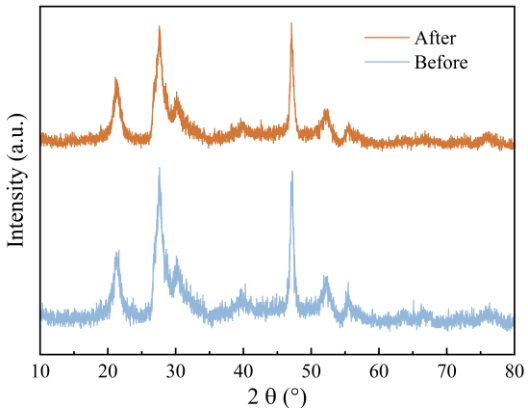

Fig. S4. XRD patterns of ZIS/CWO-3 before and after the photocatalysis.

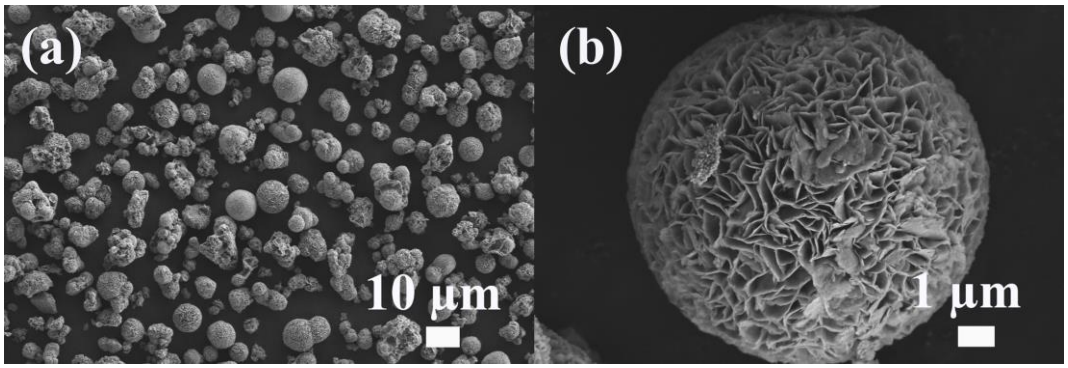

Fig. S5. SEM image of ZIS/CWO-3 after the photocatalytic reaction.

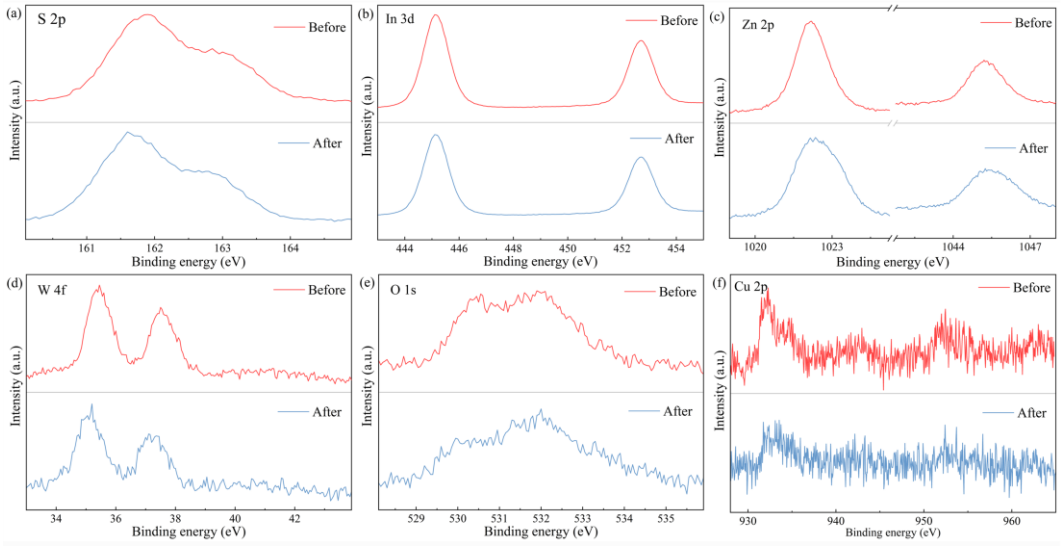

Fig. S6. XPS spectra of ZIS/CWO-3 before and after photocatalytic reaction. (a) S 2p, (b) In 3d, (c) Zn 2p (d) W 4f, (e) O 1 and (f) Cu 2p.

Fig. S7. Temperature mapping images of different samples at the initial moment.

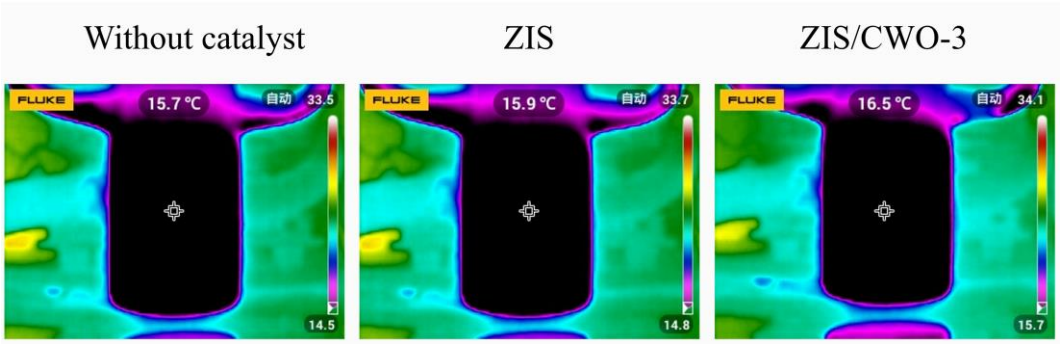

Fig. S8. Temperature mapping images of different reaction systems at the initial moment.

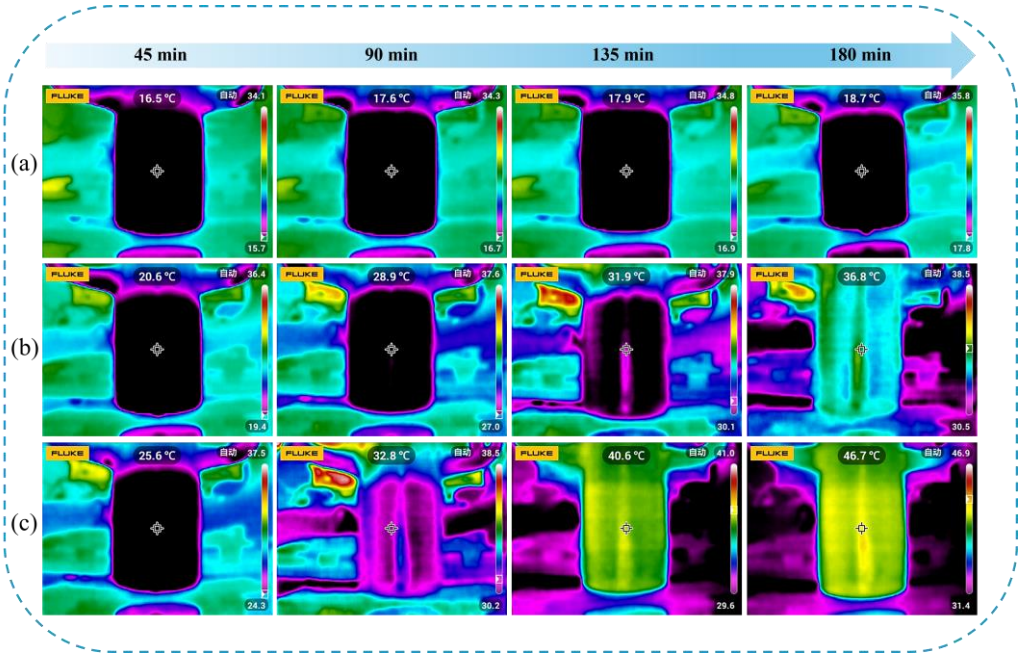

Fig. S9. Temperature mapping images under 300 W xenon lamp irradiation during the photothermal-assisted photocatalytic H_2 evolution for (a) without catalyst, (b) ZIS and (c) ZIS/CWO-3.

As shown in Fig. S10, we clarified the contributions of the heterojunction and photothermal effects by comparing the hydrogen evolution rates of ZIS/CWO-3 under different conditions: in the presence or absence of heterojunction formation, and with or without controlling the temperature to eliminate the photothermal effect. The sample that consisted of a simple physical mixture of ZIS and CWO was denoted as ZIS/CWO-Mix. To suppress the photothermal effect, an external water circulation at 10 °C was applied, denoted as ZIS/CWO-Tem. The hydrogen evolution activity was found to be very low when ZIS and CWO did not form a heterojunction. When the temperature was controlled to minimize the photothermal effect, the presence of the heterojunction still resulted in an 11.13-fold increase in the hydrogen evolution rate, whereas the photothermal effect alone led to a 9.63-fold improvement. Therefore, in the integrated ZIS/CWO-3 system, the heterojunction played a more significant role in enhancing photocatalytic H2 evolution compared to the photothermal effect.

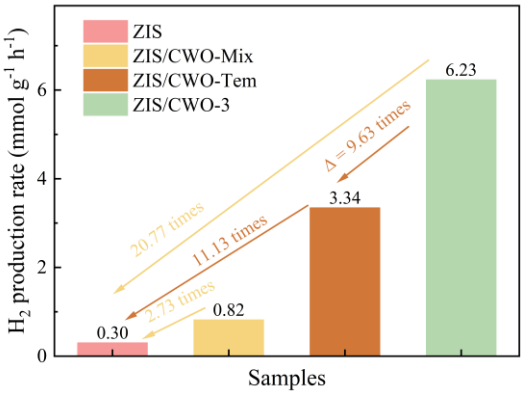

Fig. S10. Comparison of the effects of heterojunction formation and photothermal enhancement on the photocatalytic H_2 evolution activity of ZIS.

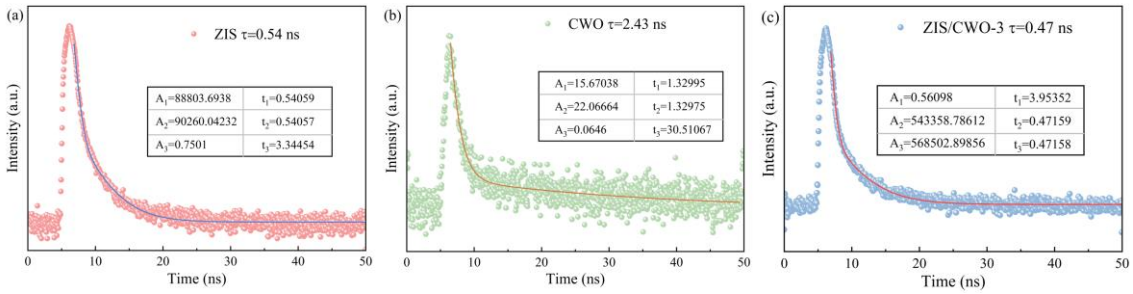

Fig. S11. TRPL spectrum of (a) ZIS, (b)CWO, and (c) ZIS/CWO-3.

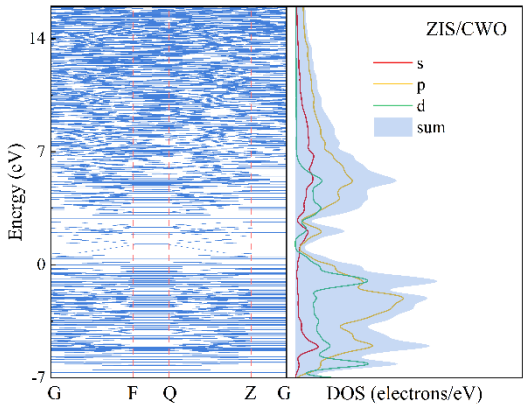

Fig. S12. Band structures and DOS of ZIS/CWO heterojunction.

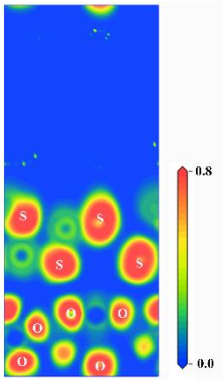

Fig. S13. ELF of ZIS/CWO heterojunction.

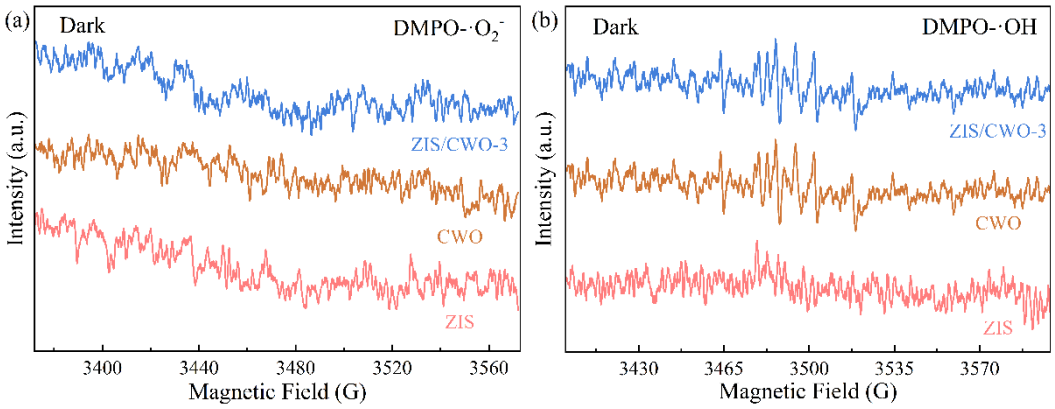

Fig. S14. (a) DMPO-•O_2^- ESR spectra and (b) DMPO- •OH ESR spectra under dark.

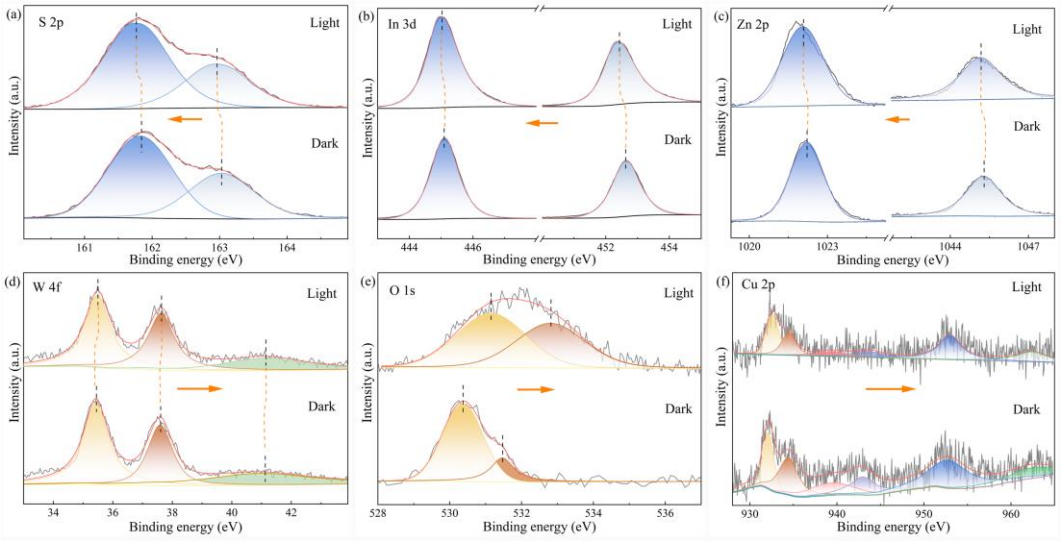

Fig. S15. In-situ irradiated high-resolution XPS spectra of ZIS/CWO-3 before and after light irradiation: (a) S 2p, (b) In 3d, (c) Zn 2p (d) W 4f, (e) O 1 and (f) Cu 2p.

Table S1. Comparison of the photocatalytic H_2 evolution activity for ZIS/CWO-3 with other ZIS-based photocatalysts.

Photocatalyst	Reactant solution	Light source	Activity (mmol h^{-1} g^{-1})	Reference
CWO/ZIS	0.35 M Na_2S and 0.25 M Na_2SO_3	300 W Xe lamp (>400 nm)	6.23	This work
SnSe/ZIS	10 vol% TEOA	300 W Xe lamp (>400 nm)	5.06	[1]
$Ni(OH)_2$/ZIS	10 vol% Lactic acid	300 W Xe lamp (>420 nm)	4.43	[2]
MoS_2/ZIS	0.35 M Na_2S and 0.25 M Na_2SO_3	300 W Xe lamp (>400 nm)	3.89	[3]
$FeWO_4$/ZIS	0.35 M Na_2S and 0.25 M Na_2SO_3	300 W Xe lamp (>400 nm)	3.53	[4]
$CuInS_2$/ZIS	0.35 M Na_2S and 0.25 M Na_2SO_3	300 W Xe lamp (>420 nm)	3.43	[5]
UiO-66/ZIS	15 vol% TEOA	300 W Xe lamp (>400 nm)	3.06	[6]
Ti_2C_3/ZIS	0.05 M Na_2S and 0.05 M Na_2SO_3	300 W Xe lamp (>400 nm)	2.60	[7]
ReS_2/ZIS	10 vol% TEOA	300 W Xe lamp (>420 nm)	1.86	[8]
$LaNiO_3$/ZIS	10 vol% TEOA	300 W Xe lamp (>400 nm)	1.60	[9]

Table S2. Comparison of the photocatalytic H_2 evolution activity for ZIS/CWO-3 with other photothermal photocatalysts.

Photocatalyst	Reactant solution	Light source	Activity (mmol h^{-1} g^{-1})	Reference
Co_9S_8@ZIS	20 vol% TEOA	300 W Xe lamp (>400 nm)	6.25	[10]
CWO/ZIS	0.35 M Na_2S and 0.25 M Na_2SO_3	300 W Xe lamp (>400 nm)	6.23	This work
$FeSe_2$/ZIS	10 vol% TEOA	300 W Xe lamp (>400 nm)	5.78	[11]
SnSe/ZIS	10 vol% TEOA	300 W Xe lamp (>400 nm)	5.66	[12]
FeS_2@ZIS	10 vol% TEOA	300 W Xe lamp (>400 nm)	5.02	[13]
$Cu_{2-x}S$@ZIS	10 vol% lactic acid	300 W Xe lamp (>420 nm)	4.65	[14]
Co_3O_4@ZIS	20 vol% TEOA	300 W Xe lamp (>400 nm)	4.52	[15]
$NiCo_2O_4$/ZIS	0.35 M Na_2S and 0.25 M Na_2SO_3	300 W Xe lamp (>400 nm)	4.51	[16]
$NiCo_2S_4$/ZIS	0.1M ascorbic acid	300 W Xe lamp (>420 nm)	1.97	[17]

References:

[1] C. Du, B. Yan, and G. Yang, Promoting photocatalytic hydrogen evolution by introducing hot islands: SnSe nanoparticles on $ZnIn_2S_4$ monolayer. Chem. Eng. J. 404 (2021) 126477. DOI: 10.1016/j.cej.2020.126477.

[2] Z. Guo, H.X. Hou, J.Y. Zhang, P.L. Cai, and J. Lin, Prominent roles of $Ni(OH)_2$ deposited on $ZnIn_2S_4$ microspheres in efficient charge separation and photocatalytic H_2 evolution. RSC Adv. 11 (2021) 12442-12448. DOI: 10.1039/d1ra01648b.

[3] Z. Zhang, L. Huang, J. Zhang, F. Wang, Y. Xie, X. Shang, Y. Gu, H. Zhao, and X. Wang, In situ constructing interfacial contact $MoS_2/ZnIn_2S_4$ heterostructure for enhancing solar photocatalytic hydrogen evolution. Appl. Catal. B.-Environ. 233 (2018) 112-119. DOI: 10.1016/j.apcatb.2018.04.006.

[4] D. Kong, X. Hu, J. Geng, Y. Zhao, D. Fan, Y. Lu, W. Geng, D. Zhang, J. Liu, H. Li, and X. Pu, Growing $ZnIn_2S_4$ nanosheets on $FeWO_4$ flowers with p-n heterojunction structure for efficient photocatalytic H_2 production. Appl. Surf. Sci. 591 (2022) 153256. DOI: 10.1016/j.apsusc.2022.153256.

[5] Z. Guan, J. Pan, Q. Li, G. Li, and J. Yang, Boosting Visible-Light Photocatalytic Hydrogen Evolution with an Efficient $CuInS_2/ZnIn_2S_4$ 2D/2D Heterojunction. ACS Sustain. Chem. Eng. 7 (2019) 7736-7742. DOI: 10.1021/acssuschemeng.8b06587.

[6] X. Peng, L. Ye, Y. Ding, L. Yi, C. Zhang, and Z. Wen, Nanohybrid photocatalysts with $ZnIn_2S_4$ nanosheets encapsulated UiO-66 octahedral nanoparticles for visible-light-driven hydrogen generation. Appl. Catal. B.-Environ. 260 (2020) 118152. DOI: 10.1016/j.apcatb.2019.118152.

[7] Y. Chen, Y. Ge, C. Wu, H. Tang, X. Luo, J. He, L. Jiang, Z. Yan, and J. Wang, Facile Synthesis of 2D/2D Ti(2)C(3)/ZnIn(2)S(4) Heterostructure for Enhanced Photocatalytic Hydrogen Generation. Int. J. Mol. Sci. 24 (2023). DOI: 10.3390/ijms24043936.

[8] X. Xiong, A. Yan, X. Zhang, F. Huang, Z. Li, Z. Zhang, and H. Weng, $ReS_2/ZnIn_2S_4$ heterojunctions

with enhanced visible-light-driven hydrogen evolution performance for water splitting. J. Alloy. Compd. 873 (2021) 159850. DOI: 10.1016/j.jallcom.2021.159850.

[9] Z. Wang, B. Su, J. Xu, Y. Hou, and Z. Ding, Direct Z-scheme $ZnIn_2S_4$/$LaNiO_3$ nanohybrid with enhanced photocatalytic performance for H_2 evolution. Int. J. Hydrogen Energ. 45 (2020) 4113-4121. DOI: 10.1016/j.ijhydene.2019.12.077.

[10] S. Wang, B.Y. Guan, X. Wang, and X. Lou, Formation of Hierarchical Co(9)S(8)@ZnIn(2)S(4) Heterostructured Cages as an Efficient Photocatalyst for Hydrogen Evolution. J. Am. Chem. Soc. 140 (2018) 15145-15148. DOI: 10.1021/jacs.8b07721.

[11] X. Liu, S. Wang, J. Cao, J. Yu, J. Dong, Y. Zhao, F. Zhao, D. Zhang, and X. Pu, Anchoring $ZnIn_2S_4$ nanosheets on cross-like $FeSe_2$ to construct photothermal-enhanced S-scheme heterojunction for photocatalytic H_2 evolution. J. Colloid Interf. Sci. 673 (2024) 463-474. DOI: 10.1016/j.jcis.2024.06.106.

[12] C. Du, B. Yan, and G. Yang, Promoting photocatalytic hydrogen evolution by introducing hot islands: SnSe nanoparticles on $ZnIn_2S_4$ monolayer. Chemical engineering journal (Lausanne, Switzerland : 1996) 404 (2021) 126477. DOI: 10.1016/j.cej.2020.126477.

[13] K. Chen, Y. Shi, P. Shu, Z. Luo, W. Shi, and F. Guo, Construction of core – shell FeS_2@$ZnIn_2S_4$ hollow hierarchical structure S-scheme heterojunction for boosted photothermal-assisted photocatalytic H_2 production. Chemical engineering journal (Lausanne, Switzerland : 1996) 454 (2023) 140053. DOI: 10.1016/j.cej.2022.140053.

[14] Y.C. Wang, M.J. Liu, C.X. Wu, J.P. Gao, M. Li, Z.P. Xing, Z.Z. Li, and W. Zhou, Hollow Nanoboxes $Cu_{2-x}S$@$ZnIn_2S_4$ Core-Shell S-Scheme Heterojunction with Broad-Spectrum Response and Enhanced Photothermal-Photocatalytic Performance. Small 18 (2022). DOI: 10.1002/smll.202202544.

[15] S. Zhang, G. Zhang, S. Wu, Z. Guan, Q. Li, and J. Yang, Fabrication of Co_3O_4@$ZnIn_2S_4$ for

photocatalytic hydrogen evolution: Insights into the synergistic mechanism of photothermal effect and heterojunction. J. Colloid Interf. Sci. 650 (2023) 1974-1982. DOI: 10.1016/j.jcis.2023.07.147.

[16] B. Wang, Y.T. Si, M.Y. Du, S.D. Zhao, J. Huang, X.Y. Zhao, S.J. Wang, K.J. Lu, and M.C. Liu, Broad-spectrum response of $NiCo_2O_4$-$ZnIn_2S_4$ p-n junction synergizing photothermal and photocatalytic effects for efficient H_2 evolution. Catal. Sci. Technol. 14 (2024) 4646-4654. DOI: 10.1039/d4cy00656a.

[17] Y. Guo, J. Sun, Y. Tang, X. Jia, Y. Nie, Z. Geng, C. Wang, J. Zhang, X. Tan, D. Zhong, J. Ye, and T. Yu, Efficient interfacial electron transfer induced by hollow-structured $ZnIn_2S_4$ for extending hot electron lifetimes. Energ. Environ. Sci. 16 (2023) 3462-3473. DOI: 10.1039/D3EE01522J.